A molecular mechanism for membrane chaperoning by a late embryogenesis abundant protein

Xiao-Han Li[1]*, Conny W.H. Yu[1], Natalia Gomez-Navarro[1], Viktoriya Stancheva[1], Hongni Zhu[4], Cristina Guibao[3], Andal Murthy[1], Boer Xie[7], Michael Wozny[1], Benjamin Leslie[3], Marcin Kaminski[6], Ketan Malhotra[1], Christopher M. Johnson[1], Martin Blackledge[2], Balaji Santhanam[1,3], Douglas R. Green[6], Junmin Peng[7], Wei Liu[5], Jinqing Huang[4], Elizabeth A. Miller[1]*, Stefan M.V. Freund[1], M. Madan Babu[1,3]*

[1] MRC Laboratory of Molecular Biology, Francis Crick Avenue, Cambridge, CB2 0QH, United Kingdom

[2] Université Grenoble Alpes, CNRS, Commissariat à l'Energie Atomique et aux Energies Alternatives, Institut de Biologie Structurale, 38000 Grenoble, France

[3] Department of Structural Biology and Center for Data Driven Discovery, St. Jude Children's Research Hospital, Memphis, TN, USA

[4] Department of Chemistry, The Hong Kong University of Science and Technology, Clear Water Bay, Hong Kong, China

[5] State Key Laboratory of Synthetic Chemistry, Department of Chemistry, The University of Hong Kong, Pokfulam Road, Hong Kong, China

[6] Department of Immuology, St. Jude Children's Research Hospital, Memphis, TN, USA

[7] Center for Proteomics and Metabolomics, St. Jude Children's Research Hospital, Memphis, TN, USA

*Corresponding authors. Email: xli@mrc-lmb.cam.ac.uk, emiller@mrc-lmb.cam.ac.uk, madan.babu@stjude.org

Summary

Environmental stress can result in substantial damage to proteins, membranes, and genetic material, impacting organismal survival[1-3]. Stress tolerance can be conferred by intrinsically disordered proteins (IDPs)[4] that lack stable tertiary structure. IDPs from the large family of late embryogenesis abundant (LEA) proteins confer a fitness advantage when heterologously expressed[5,6]. Such protection suggests a general molecular function leading to stress tolerance, although the mechanisms remain unclear. Here, we report that a tardigrade LEA protein that confers stress tolerance in yeast acts as a molecular chaperone for the mitochondrial membrane. This protein, named HeLEA1, localizes to the mitochondrial matrix, and harbors conserved LEA sequence motifs that undergo dynamic disorder-to-helical transition upon binding to negatively charged membranes. Yeast expressing HeLEA1 show increased mitochondrial membrane fluidity, increased membrane potential, and enhanced tolerance to hyperosmotic stress under non-fermentative growth without significantly altering mitochondrial lipid composition or triggering a generic stress response. We demonstrate that membrane binding ameliorates excess surface tension, possibly by stabilizing lipid packing defects. Evolutionary analysis suggests that HeLEA1 homologs localize to different membrane-bound organelles and share similar sequence and biophysical features. We suggest that membrane chaperoning by LEA proteins represents a general biophysical solution that can operate across the domains of life.

Introduction

47

48 Organisms often face environmental challenges that can affect their survival. Such

49 challenges include extreme temperatures (heat or cold shock), water stress (desiccation

50 or freezing) as well as altered osmotic pressure, and can result in substantial damage to

51 proteins, membranes, and genetic material[1-3]. To survive these conditions, organisms

52 adopt multiple strategies. Whereas large animals can physically move from harsh

53 environments, organisms such as plants, microbes, and small animals that cannot move

54 quickly have evolved cellular mechanisms to combat abiotic stress. One common

55 response to diverse stresses is the expression of proteins that can increase levels of

56 intracellular osmolytes and chemical chaperones such as trehalose, betaine, glycine[7,8],

57 and/or proteins that have a direct protective role on cellular components[9,10]. A subset of

58 the latter category includes proteins with no defined tertiary structure, typically referred to

59 as intrinsically disordered proteins (IDPs)[4]. For instance, small heat shock proteins

60 (sHSPs) function as chaperones that protect other proteins from misfolding and

61 aggregation[11-13].

62 The late embryogenesis abundant (LEA) proteins are among the earliest IDP families

63 discovered as combating multiple environmental stresses[5]. LEA proteins feature multiple

64 low-complexity sequence repeats[14], and are widely expressed in plants but also found in

65 microorganisms and some invertebrates[5]. LEA proteins confer tolerance in the face of

66 multiple types of stress, even when heterologously expressed[15-17]. *In vitro* experiments

67 have suggested that LEA proteins and other IDPs adopt a vitrified state or form fibrous

68 gels upon stress that might chaperone cellular proteins[18,19]. Additional evidence also

69 implicates a role for IDPs in modulating vitrification of small molecules like sugars[20,21].

70 Moreover, LEA proteins have also been linked to broader protective functions, including

71 enhancing function of membrane-bound organelles[22,23], or acting as "molecular shields" to

72 protect proteins against aggregation[24]. Consistent with a function that directly impacts

73 membranes, *in vitro* studies have suggested that LEA proteins may protect liposomes

74 from deformation during desiccation or freezing[25-27]. Despite extensive efforts, clear

75 molecular functions of LEA proteins and mechanisms by which IDPs more broadly confer

76 stress tolerance remain poorly understood. Molecular insight into such function is

77 important in the context of the evolutionary conservation of such proteins and their roles in

78 stress-protection.

79 Here we set out to define conserved mechanisms by which IDPs confer stress tolerance

80 using a multidisciplinary approach. A combination of cellular, biophysical, structural, and

81 evolutionary analyses suggests that a tardigrade LEA protein, named HeLEA1,

82 chaperones mitochondrial membranes. HeLEA1 belongs to a family of LEA proteins that

83 are predicted to localize to various membrane-bound organelles. Evolutionarily conserved

84 LEA motifs undergo dynamic interactions with negatively charged lipids to protect the

85 bilayer from thermal fluctuation and excess membrane tension. We propose that natural

86 selection has preserved sequence features that drive both a disordered state and a

87 membrane-bound structured state to confer function as a molecular chaperone for lipid

88 bilayers in different sub-cellular organelles across diverse organisms.

89

HeLEA1 is an evolutionarily conserved IDP that localizes to the mitochondria matrix

90

91 Previous work has shown that heterologous expression of tardigrade IDPs in unicellular

92 organisms such as *Saccharomyces cerevisiae* enhances their tolerance to desiccation[18].

93 Inspired by this, we performed a comprehensive sequence search with HMMer[28] to

94 identify all remote homologs of the four tardigrade proteins demonstrated to confer

95 desiccation tolerance when expressed in other organisms[18]. We identified 144 homologs

96 of these four proteins, subjected them to an all-against-all sequence comparison and

97 clustered them using the Enzyme Function Initiative similarity tool[29]. Our analysis

98 identified two clusters: three of the four queried sequences belong to the cytosolic

99 abundant heat soluble (CAHS) protein family, which contains only tardigrade proteins

100 (**Extended Data Fig. 1 and Extended Data Table 1**; 48 sequences from three tardigrade

101 species). The fourth protein belongs to a different family that is evolutionarily conserved

102 and clusters with a group of LEA proteins (Pfam: PF02987, Group 3[30], LEA_4[31], or Group

103 6[32] according to different classifications) (**Extended Data Fig. 1-2, Extended Data Table

104 2**; 96 sequences from 44 species, including two tardigrade species). We renamed this

105 tardigrade protein, which was previously classified as a CAHS protein (UniProtID:

106 P0CU49) as HeLEA1 (i.e., LEA protein from *Hypsibius exemplaris*).

107 HeLEA1 homologs are found across diverse species, including bacteria, fungi, plants,

108 and invertebrates, but not vertebrates (**Extended Data Fig.2 and Extended Data Table

109 2**). This distribution suggests conservation of HeLEA1 over millions of years of evolution in

110 organisms that require molecular responses to stress. Computational analysis of these

111 sequences suggested that different family members might localize to distinct subcellular

112 compartments and organelles, including the nucleus, chloroplast, and mitochondria (**Fig.

113 1a and Extended Data Table 3**). HeLEA1 itself was predicted to target to mitochondria

114 via a cleavable 38-residue mitochondrial-targeting sequence (MTS) at its N-terminus

115 (**Extended Data Fig. 3**). Alignment between HeLEA1 and representative homologs

116 revealed reasonable sequence similarity, but also long gaps (**Extended Data Fig. 4**). This

117 is probably due to the high propensity for HeLEA1 homologs to be intrinsically disordered

118 (83 of 96 with a mean IUPred disorder score > 0.5) (**Fig. 1b, Extended Data Fig. 5**), and

119 the tendency for LEA proteins broadly to feature multiple copies of sequence repeats that

120 vary in number. We performed a motif search using MEME algorithm[33] across 96

121 homologs and found conserved LEA protein motifs distributed along the HeLEA1

122 sequence with high confidence (**Fig. 1b-Fig. 1c**). We therefore consider HeLEA1 an ideal

123 model to investigate conserved molecular mechanisms by which LEA-related IDPs confer

124 stress tolerance.

125 To test the subcellular localization of HeLEA1, we tagged full-length HeLEA1

126 (HeLEA1$_{FL}$) with GFP at the C-terminus and expressed the fusion construct in

127 *Saccharomyces cerevisiae*, which lacks HeLEA1 orthologs. HeLEA1$_{FL}$ co-localized with a

128 mitochondrial marker, Tom20[34], whereas a mutant that lacked the putative MTS

129 (HeLEA1$_{\Delta MTS}$) accumulated in the cytoplasm. Moreover, appending the predicted MTS to

130 GFP resulted in mitochondrial localization, suggesting the predicted MTS is both

4

131 necessary and sufficient for mitochondrial targeting (**Fig. 1d**). Consistent with delivery to
132 the mitochondrial matrix, immunoblot analysis of yeast lysates from mid-log phase cells
133 expressing HA-tagged HeLEA1$_{FL}$ or HeLEA1$_{\Delta MTS}$ revealed multiple bands for HeLEA1$_{FL}$,
134 the smaller of which co-migrated with the single HeLEA1$_{\Delta MTS}$ band (**Fig. 1e**). In cells from
135 stationary phase, HeLEA1$_{FL}$ migrated as a single band with slightly lower apparent
136 molecular weight than HeLEA1$_{\Delta MTS}$ (**Extended Data Fig. 6**). These observations are
137 consistent with HeLEA1$_{FL}$ being targeted to the mitochondrial matrix, then cleaved by the
138 mitochondrial processing peptidase (MPP), followed by a further processing step. Indeed,
139 when HeLEA1$_{FL}$ was expressed in an *oct1Δ* strain that lacks a mitochondrial matrix
140 peptidase that acts downstream of MPP[35], more of the larger processing intermediates
141 accumulated, suggesting matrix localized Oct1 is involved in processing of HeLEA1$_{FL}$
142 (**Fig. 1f**). We conclude that HeLEA1 is a mitochondrial matrix protein and that its mature
143 form is HeLEA1$_{\Delta MTS}$ (hereafter referred to as HeLEA1), with potential further processing at
144 an Oct1 cleavage site (**Fig. 1g**).

145   To characterize the secondary structure of HeLEA1, we expressed and purified the
146 recombinant protein from bacteria and investigated its secondary structure using circular
147 dichroism (CD). The CD spectra of HeLEA1 showed characteristic signatures of random
148 coil, suggesting the protein is largely disordered (**Extended Data Fig. 7**). To gather
149 residue-specific structural information, we further characterised isotopically labelled
150 HeLEA1 by solution-state nuclear magnetic resonance (NMR) spectroscopy. Using a
151 combination of standard triple resonance experiments and (^{1}H-start) ^{13}C-detect
152 experiments, backbone resonances for 191 out of 200 residues (90%) in HeLEA1 were
153 assigned at 278 K (**Fig. 1h, Extended Data Fig. 8**). Two features stood out in the ^{1}H$_N$-^{15}N
154 2D HSQC spectra: (a) very narrow dispersion of amide proton chemical shifts, and (b)
155 clustering of the backbone ^{1}H$_N$,^{15}N resonances in the 2D spectrum according to amino
156 acid type. These features define HeLEA1 as an intrinsically disordered protein in
157 solution.[36]

158   In addition to the general feature of predicted disorder in solution (**Extended Data Fig.
159 5**) and conserved LEA motifs, our sequence search suggested that some HeLEA1
160 homologs harbour sequence motifs with similarity to the apolipoprotein superfamily (Pfam)
161 (**Extended Data Fig. 9**). Additionally, a PhyRE2[37] structural similarity search probing the
162 PDB database with the HeLEA1 sequence yielded hits with apolipophorin-III, α-synuclein
163 and HSP12 (**Extended Data Fig. 10**), all of which associate with membranes via
164 amphipathic helices[38]. We therefore devised a computational pipeline to identify potential
165 3-11 helical elements (minimum length = 7 residues, with aligned amphipathic interface)
166 that may interact with lipids according to previously reported criteria for predicting
167 continuous amphipathic helical elements[39] and apolipoprotein motifs[40,41] (**Extended Data
168 Fig. 11**). We identified eight putative amphipathic 3-11 helical elements of various lengths
169 in HeLEA1 (H1–H8, **Fig. 1i, Extended Data Fig. 12**). These elements are enriched in
170 weakly hydrophobic residues (alanines and threonines) and exhibit a small hydrophobic
171 surface (3–5 of the 11 projected positions is hydrophobic). Moreover, four of the eight
172 helices (H2, H6–H8) displayed strong enrichment of positively charged residues (lysines
173 and arginines) at the boundary of the hydrophobic and hydrophilic surfaces, and

174   enrichment of negatively charged residues (glutamates and aspartates) in the hydrophilic
175   surface. The other helices (H1, H3–H5) also exhibit these features, albeit weakly. The
176   biophysical prediction corresponds well with PSIPRED (**Extended Data Fig. 13**) and
177   AlphaFold2 prediction[42] (**Extended Data Fig. 12, Fig. 1i**). The low pLDDT score of the
178   AlphaFold2 prediction suggests a low confidence global structure (**Extended Data Fig.
179   12**), probably due to the disordered nature of HeLEA1 causing difficulty with sequence
180   alignment (**Extended Data Fig. 4, Extended Data Fig. 5**). Nonetheless, local secondary
181   structural elements predicted by AlphaFold match our biophysical prediction (**Extended
182   Data Fig. 12**). The low confidence in stably-folded long amphipathic helices but
183   agreement on local secondary structure predictions would be consistent with a dynamic
184   disorder-to-helical transition in HeLEA1, a common feature of IDPs binding to
185   membranes[43-46] that is also shared by some LEA proteins[6].

186

187   **Conserved LEA motifs remain conformationally dynamic during the early stages of**
188   **disorder-to-helical transition of HeLEA.**

189   IDPs are frequently proposed to function as an entropic buffer, maintaining a degree of
190   disorder even when adopting a functionally relevant conformational state[4]. Our
191   computational analysis of HeLEA1 suggests specific sequence elements that can adopt
192   both disordered and structurally defined states, largely consisting of amphipathic elements
193   (**Fig. 1i**). To gain structural insight into these elements, we sought to probe HeLEA1's
194   conformational states and backbone dynamics in solution, using trifluoroethanol (TFE)
195   perturbation. TFE is frequently used in protein folding studies to mimic conditions under
196   which transient helical components of the conformational ensemble are stabilized[47].
197   Circular dichroism (CD) revealed that TFE indeed induced helicity of HeLEA1 in a
198   concentration-dependent manner (**Fig. 2a**). We subsequently performed integrative
199   structural analysis of HeLEA1 in either 0% or 10% TFE, conditions under which HeLEA1
200   remained predominantly disordered (**Fig. 2a inset**). Any observed residue-specific
201   differences for these two conformational states should provide insight into disorder-to-
202   helical transitions for each amphipathic element. In general, the biophysical properties of
203   HeLEA1 were experimentally investigated by SAXS and NMR, and the *ASTEROIDS*
204   algorithm[48,49] was used to determine the conformational ensemble that best described all
205   experimental data (**Extended Data Fig. 14**). We found that 10% TFE mildly increased the
206   global helical propensity, with certain regions of H1 (51-54), H2 (57-62), H4 (114-120), H7
207   (183-187) exhibiting a significant increase in helical conformation (**Fig. 2b, Extended
208   Data Fig. 15**). The radii of gyration (R_g) of HeLEA1 in 0% TFE and 10% TFE were larger
209   than the R_g predicted for a statistical random coil (**Fig. 2c**) and adding 10% TFE resulted
210   in a small decrease of R_g compared to the 0% TFE condition (**Fig. 2c, Extended Data
211   Table 4, Extended Data Fig. 16**). These results correspond well with HeLEA1 occupying
212   a largely expanded disordered state, but with significant increase in helical propensity
213   within short local segments at the early stage of disorder-to-helical transition (**Fig. 2d**).

214   We next probed protein backbone dynamics by ^{15}N NMR relaxation measurements as
215   HeLEA1 transits from disorder-to-helical conformation. [15]N{[1]H} heteronuclear nuclear

6

216 Overhauser effect (hetNOE) experiments probe fast (picoseconds) backbone dynamics
217 but revealed only a small global increase in 10% TFE, potentially indicating a modest
218 increase in overall rigidity (**Extended Data Fig. 17**). Accordingly, a modest decrease was
219 observed for ^{15}N R_1 ($1/T_1$) longitudinal relaxation rates (**Fig. 2e**). In contrast, ^{15}N R_2 ($1/T_2$)
220 transverse relaxation rates displayed a dramatic increase under 10% TFE conditions (**Fig.**
221 **2e**). ^{15}N R_2 rates sample backbone dynamics at multiple time scales and are exquisitely
222 sensitive to 'segmental motions' associated with the formation of transiently populated
223 secondary structural elements. Sequence elements with significantly increased ^{15}N R_2
224 rates correlate with regions exhibiting increased helicity (**Fig. 2b**). These results support
225 the model that a disorder-to-helical transition is initiated via the population of local
226 secondary structure elements. This results in a global decrease in backbone flexibility and
227 shifts the overall conformational ensemble towards higher helical propensity. Importantly,
228 the regions that mapped to evolutionarily conserved LEA motifs did not completely overlap
229 with regions of higher helical propensity (**Fig. 2b**). The localizations of these
230 conformationally dynamic motifs imply that maintaining a high conformational-entropy
231 state in the conserved regions may be important in the function of LEA proteins, while the
232 neighbouring helical-prone regions may buffer the cost of conformational entropy during
233 the disorder-to-helical transition. (**Fig. 2f**).

234

235 **HeLEA1 stabilizes negatively charged membranes through dynamic disorder-helical**
236 **transition**

237 Our cellular localization and conformational dynamics data suggest that in its
238 physiological setting, HeLEA1 undergoes a disorder-to-helical conformational change
239 upon binding to the inner mitochondrial membrane (IMM). We therefore directly tested
240 whether HeLEA1 can be recruited to membranes using a liposome flotation assay. Since
241 the IMM is enriched in negatively charged lipids, and the amphipathic elements in HeLEA1
242 are enriched in positively charged residues (**Extended Data Fig. 12, Fig. 2f**), we tested
243 HeLEA1 recruitment to small unilamellar vesicles (SUVs) made with either negatively
244 charged POPS or neutral POPC. At physiological salt concentrations, HeLEA1 stably
245 associated with POPS, but not POPC SUVs (**Fig. 3a**). Increasing the salt concentration,
246 which suppresses electrostatic interactions but encourages hydrophobic interactions,
247 abolished binding of HeLEA1 to negatively charged liposomes and promoted weak
248 association with neutral liposomes (**Fig. 3a**). Thus, HeLEA1 can bind negatively charged
249 membranes primarily through electrostatic interactions but may interact weakly with
250 neutral lipids via hydrophobic interactions.

251 We next determined whether membrane binding induces structural changes similar to
252 those observed with TFE. We titrated HeLEA1 with SUVs containing various ratios of
253 neutral lipids to negatively charged lipids and monitored the changes in protein secondary
254 structure by CD. We observed increased helicity of HeLEA1 with increasing
255 concentrations of negatively charged SUVs (**Fig. 3b**) and proportional to the fraction of
256 negatively charged lipids (**Fig. 3c**). The CD spectra of the POPS titration revealed an
257 isodichroic point at 204 nm, which is characteristic of a classic disorder-to-helical
258 transition[50]. Deconvolution of the CD titration curves with Bestsel[51] suggested that at least

259 60% of the residues in lipid-bound HeLEA1 are in a helical conformation, corresponding
260 well with predictions of possible secondary structures and TFE-induced disorder-to-helical
261 transition (**Fig. 1i, Fig. 2a**). Moreover, we observed complete reversibility of such
262 membrane-induced disorder-to-helical transition without cooperativity in thermal melting
263 and refolding experiments (**Extended Data Fig. 18**). Such reversibility corresponds well
264 with the highly dynamic behaviour of HeLEA1 during its structural transition as mapped by
265 TFE titration. Importantly, the positional distribution of the conserved dynamic LEA motifs
266 correlates with a weak local hydrophobic moment and the presence of negative charge
267 clusters, featuring a low lipid discrimination factor and indicating weak protein-lipid
268 interaction (**Extended Data Fig. 19**). These features are conserved in amphipathic
269 elements in HeLEA1 homologs, compared to similar amphipathic elements observed in
270 apolipoproteins that is known to stably bind to lipids for structural scaffolding (**Extended
271 Data Fig. 20**). These observations highlight the importance of weak and dynamic lipid
272 binding in the functioning of HeLEA1.

273 We therefore postulated that weak binding of HeLEA1 to negatively charged
274 membranes confers chaperone-like activity to modulate the biophysical properties of the
275 bilayer. We first tested this model by investigating the temperature-dependent lipid phase
276 transition of negatively charged synthetic membranes using differential scanning
277 calorimetry (DSC) in the presence or absence of HeLEA1. DSC measures heat flux
278 towards the sample as a result of changing temperature. A lipid bilayer will have a
279 characteristic DSC peak triggered by phase transition from an ordered phase to a liquid
280 disordered phase as packing of fatty acids becomes disordered with increasing
281 temperature. In the absence of HeLEA1, POPS SUVs displayed a somewhat complex
282 phase transition profile over a broad temperature range (**Fig. 3d**), as previously
283 reported[11]. Addition of sub-stoichiometric amounts of HeLEA1 (1:200 molar ratio of
284 protein:POPS) suppressed phase transition at low temperatures (arrow in **Fig. 3d**) and
285 increased the dominant phase transition temperature (DSC peak position) (dashed lines in
286 **Fig. 3d**). Experiments using SUVs composed of 100% DMPS, a lipid with saturated fatty
287 acid chains, yielded similar results, whereas the behaviour of SUVs made of neutral lipids
288 remained mostly unchanged in the presence of HeLEA1 (**Extended Data Fig. 21**). These
289 results suggest that HeLEA1 can stabilize membranes from thermally induced fluctuations
290 of bilayers independent of the saturation state of lipid side chains.

291 We next tested if HeLEA1 can also modulate mechanical properties of membranes
292 using Langmuir-monolayer methodology[52], in which the relationship between the surface
293 pressure and area of a lipid monolayer is determined as compression isotherms
294 (**Extended Data Fig. 22**). The resulting curves are used to compute the compression
295 modulus ($C_S{}^{-1}$), which reports on the stiffness of the lipid monolayer: lower $C_S{}^{-1}$ values
296 correspond to softer and more compressible membranes with increased fluidity[53]. The
297 presence of 3nM HeLEA1, which translates to a protein-to-lipid ratio of 1:50, substantially
298 decreased $C_S{}^{-1}$ (i.e., increased membrane fluidity) for POPS monolayers (**Fig. 3e**) but
299 marginally changed the $C_S{}^{-1}$ for POPC monolayers (**Extended Data Fig. 23**), in good
300 agreement with its preferred recruitment to negatively charged phospholipids. Notably, this
301 effect was most prominent in the physiological range of surface pressures, i.e., 25–35

302   mN/m (**Fig. 3e**, gray box)[53]. The mean $C_S{}^{-1}$ of the POPS monolayer changed from
303   85.4±5.8 mN/m to 54.8±6.6 mN/m at physiological membrane surface pressure,
304   suggesting a significant increase in membrane fluidity[53]. At high surface pressure, the $C_S{}^{-1}$
305   of the POPS monolayer with HeLEA1 was restored to that without HeLEA1, suggesting
306   that HeLEA1 fall out of the lipid monolayer, suggesting a reversible and dynamic protein-
307   lipid interaction.

308   Together, our biochemical data with synthetic bilayers are consistent with a role for
309   HeLEA1 as a conserved molecular chaperone for lipid bilayers that promotes stabilization
310   and modulation of membrane fluidity. The evolutionarily conserved dynamic disorder-
311   helical transition features in HeLEA1 contribute to its chaperone function (**Fig. 3f**).

HeLEA1 expression enhances tolerance to hyperosmotic stress on non-fermentable carbon sources

315   To further explore HeLEA1 activity under more physiological conditions, we first tested
316   recruitment to giant unilamellar vesicles (GUVs) that mimic the IMM composition[54]. We
317   encapsulated N-terminally fluorescently labelled HeLEA1 inside the GUVs and imaged
318   both lipid and protein by confocal imaging. HeLEA1 colocalized with the GUV membrane
319   (**Fig. 4a**), suggesting that HeLEA1 binds membranes of a physiologically relevant
320   composition. We next aimed to observe HeLEA1's function on mitochondria more directly.
321   We generated a yeast strain that expresses HeLEA1$_{FL}$ under a strong constitutive
322   promoter, purified mitochondria and stained them with diphenylhexatriene (DPH). DPH
323   fluoresces in a hydrophobic environment, and its anisotropy reports on membrane fluidity,
324   where low anisotropy (faster tumbling) corresponds to a more fluid membrane (less
325   ordered lipids). Mitochondria from HeLEA1-expressing cells showed decreased DPH
326   anisotropy, i.e., increased membrane fluidity, compared to wild type cells (**Fig. 4b**). This
327   change in fluidity is unlikely to be driven by changes to the lipid composition because
328   principal component analysis of lipidomics experiments from isolated mitochondria
329   revealed no significant difference in composition between these two conditions (**Extended
330   Data Fig. 24**).

331   Hyperosmotic stress is commonly associated with upregulation of stress-related IDPs
332   including LEA proteins[2,55,56], and altered mitochondrial function[57,58]. We therefore tested if
333   HeLEA1 could confer enhanced tolerance to salt stress (0.5M NaCl). Strikingly, HeLEA1$_{FL}$
334   expression conferred a substantial growth advantage only when grown on non-
335   fermentable glycerol media at 37 °C, where cell growth is dependent on mitochondrial
336   function[59]. In contrast, on glucose media, where mitochondrial biogenesis is repressed
337   and mitochondrial function is not essential, there was no growth advantage (**Fig. 4c**). We
338   observed similar effects in cells grown on lactate, another non-fermentable carbon source,
339   and using other hyperosmotic stress conditions including 0.5 M KCl and 1.0 M sorbitol
340   (**Fig. 4c, Extended Data Fig. 25**). Similar phenotypes were also observed when
341   HeLEA1$_{FL}$ was expressed under a weaker promoter (**Extended Data Fig. 26**).
342   Overexpression of GFP with the HeLEA1 MTS did not confer stress protection to the
343   same extent (**Extended Data Fig. 27**), suggesting the phenotype is not caused by
344   mitochondrial import stress. Similarly, altered lipid composition of the mitochondria is

345 unlikely to explain the growth phenotypes since we did not observe significant changes in

346 mitochondrial lipid composition in the presence or absence of HeLEA1$_{FL}$ under glycerol

347 growth (**Extended Data Fig. 28**). Instead, we observed that HeLEA1$_{FL}$ expression

348 conferred a higher mitochondrial membrane potential. For this, we stained mid-log phase

349 cells growing in glycerol with TMRM, a fluorescent dye whose accumulation in

350 mitochondria is dependent on membrane potential. We normalized TMRM fluorescence to

351 mitochondrial abundance using TOM20-eGFP. HeLEA1$_{FL}$ expression resulted in higher

352 TMRM fluorescence consistent with increased mitochondrial membrane potential (**Fig.**

353 **4d**). As HeLEA1 does not have any homologs identified in yeast (**Extended Data Table**

354 **2**), these phenotypes because of heterologous expression of HeLEA1 strongly support

355 that membrane chaperoning by HeLEA1 promotes mitochondrial function may serve as a

356 general biophysical mechanism for stress tolerance.

357

Discussion

359 Since the discovery of LEA proteins from cotton seeds, the relevance of these IDPs for

360 stress tolerance has been demonstrated in multiple organisms and model systems,

361 including tardigrades[23,60] and arthropods[12,15,61]. However, the molecular mechanism by

362 which these stress-tolerance proteins exert their protective function has remained less

363 clear. Using the tardigrade HeLEA1 protein as a model, we performed a detailed

364 characterization at multiple scales (atomic, molecular, subcellular, cellular, and

365 evolutionary) to uncover a possible general molecular mechanism by which the IDPs of

366 the LEA family confer stress tolerance.

367   We showed that HeLEA1 is an IDP that localizes to mitochondria and undergoes a

368 disorder-to-helical transition in the presence of negatively charged lipids. The high

369 conformational entropy of the intrinsically disordered state stabilizes HeLEA1 in solution,

370 whereas HeLEA1 folding upon binding to negatively charged lipids trades a loss of

371 conformational entropy for enthalpic gain from electrostatic interactions, exposing the

372 hydrophobic surfaces of the weakly amphipathic helical elements. This mechanism

373 explains the importance of the conserved LEA motifs (**Fig. 2f**), which confer reversible

374 association with lipids. Such dynamic interactions may buffer local changes in the surface

375 tension and packing defects of membranes (**Fig. 3f**). Because the IMM is enriched in

376 negatively charged lipids, including cardiolipin[62,63], the dynamic membrane-binding

377 process of HeLEA1 may thereby encourage the diffusion of transmembrane proteins[64] in

378 the IMM as well as buffering changes in membrane tension during stress and membrane

379 protein biogenesis. The notion is further supported by evidence where increased

380 membrane fluidity of mitochondria by altering unsaturation side chains enhance their

381 function[65].

382   Our observations that HeLEA1 only confers significant hyperosmotic stress tolerance

383 on non-fermentable carbon source, when mitochondrial function is essential, suggest that

384 the molecular function of an IDP (i.e., its biophysical properties and behaviour) can be

385 robust, while its cellular function (i.e., effect on mitochondrial activity) is context

386 dependent. Our evolutionary analysis suggests that amphipathic elements in HeLEA1

387 homologs with different predicted targeting signals display trade-offs between fraction of
388 basic residues and hydrophobicity, while keeping the hydrophobic moments unchanged
389 (**Extended Data Fig. 30**). We propose that the molecular function of weak lipid binding
390 (i.e. low hydrophobic moments) is conserved, but the mechanism for lipid recognition
391 (electrostatic-driven versus hydrophobic-driven) is fine-tuned according to diverse
392 subcellular localizations, where different membrane-bound organelles differ in their lipid
393 compositions[66,67]. Proteins with distant structural similarity to HeLEA1, such as
394 apolipoproteins, may have evolved away from the need to protect organelles from
395 environmental stresses and acquired new functions, such as stabilization of lipoprotein
396 particles in mammals. Accordingly, their sequences evolved to change their biophysical
397 properties from dynamic and disordered to stable and folded (**Extended Data Fig. 19**).

398   The expression of a tardigrade protein that confers stress tolerance in yeast highlights
399 the generic biophysical basis for stress tolerance through functional enhancement of
400 membrane-bound organelles. Therefore, HeLEA1 homologs may confer abiotic stress
401 tolerance by acting as membrane chaperones, i.e., maintaining the membrane fluidity of
402 membrane-bound organelles and facilitating proper biological functions of their associated
403 membrane proteins (**Fig. 5**). We suggest that such a biophysical mechanism may
404 represent a simple and evolvable solution that can confer stress tolerance across the
405 different domains of life.

406

References:

408 1   Zhu, J. K. Abiotic Stress Signaling and Responses in Plants. *Cell* **167**, 313-324,
409   doi:10.1016/j.cell.2016.08.029 (2016).
410 2   Calahan, D., Dunham, M., DeSevo, C. & Koshland, D. E. Genetic analysis of
411   desiccation tolerance in Sachharomyces cerevisiae. *Genetics* **189**, 507-519,
412   doi:10.1534/genetics.111.130369 (2011).
413 3   Lebre, P. H., De Maayer, P. & Cowan, D. A. Xerotolerant bacteria: surviving
414   through a dry spell. *Nat Rev Microbiol* **15**, 285-296, doi:10.1038/nrmicro.2017.16
415   (2017).
416 4   van der Lee, R. *et al.* Classification of intrinsically disordered regions and proteins.
417   *Chem Rev* **114**, 6589-6631, doi:10.1021/cr400525m (2014).
418 5   Hand, S. C., Menze, M. A., Toner, M., Boswell, L. & Moore, D. LEA proteins during
419   water stress: not just for plants anymore. *Annu Rev Physiol* **73**, 115-134,
420   doi:10.1146/annurev-physiol-012110-142203 (2011).
421 6   Hernandez-Sanchez, I. E. *et al.* LEAfing through literature: Late embryogenesis
422   abundant proteins coming of age - achievements and perspectives. *J Exp Bot*,
423   doi:10.1093/jxb/erac293 (2022).
424 7   Csonka, L. N. Physiological and genetic responses of bacteria to osmotic stress.
425   *Microbiol Rev* **53**, 121-147 (1989).
426 8   Tarczynski, M. C., Jensen, R. G. & Bohnert, H. J. Stress protection of transgenic
427   tobacco by production of the osmolyte mannitol. *Science* **259**, 508-510,
428   doi:10.1126/science.259.5094.508 (1993).
429 9   Schopf, F. H., Biebl, M. M. & Buchner, J. The HSP90 chaperone machinery. *Nat*
430   *Rev Mol Cell Biol* **18**, 345-360, doi:10.1038/nrm.2017.20 (2017).

431 10   Jarosz, D. F. & Lindquist, S. Hsp90 and environmental stress transform the
432   adaptive value of natural genetic variation. *Science* **330**, 1820-1824,
433   doi:10.1126/science.1195487 (2010).
434 11   Welker, S. *et al.* Hsp12 is an intrinsically unstructured stress protein that folds upon
435   membrane association and modulates membrane function. *Mol Cell* **39**, 507-520,
436   doi:10.1016/j.molcel.2010.08.001 (2010).
437 12   Pouchkina-Stantcheva, N. N. *et al.* Functional divergence of former alleles in an
438   ancient asexual invertebrate. *Science* **318**, 268-271, doi:10.1126/science.1144363
439   (2007).
440 13   Theillet, F. X. *et al.* Physicochemical properties of cells and their effects on
441   intrinsically disordered proteins (IDPs). *Chem Rev* **114**, 6661-6714,
442   doi:10.1021/cr400695p (2014).
443 14   Battaglia, M., Olvera-Carrillo, Y., Garciarrubio, A., Campos, F. & Covarrubias, A. A.
444   The enigmatic LEA proteins and other hydrophilins. *Plant Physiol* **148**, 6-24,
445   doi:10.1104/pp.108.120725 (2008).
446 15   Li, S. *et al.* Late embryogenesis abundant proteins protect human hepatoma cells
447   during acute desiccation. *Proc Natl Acad Sci U S A* **109**, 20859-20864,
448   doi:10.1073/pnas.1214893109 (2012).
449 16   Imai, R., Chang, L., Ohta, A., Bray, E. A. & Takagi, M. A lea-class gene of tomato
450   confers salt and freezing tolerance when expressed in Saccharomyces cerevisiae.
451   *Gene* **170**, 243-248, doi:10.1016/0378-1119(95)00868-3 (1996).
452 17   Anderson, J. M. & Hand, S. C. Transgenic expression of late embryogenesis
453   abundant proteins improves tolerance to water stress in Drosophila melanogaster.
454   *J Exp Biol* **224**, doi:10.1242/jeb.238204 (2021).
455 18   Boothby, T. C. *et al.* Tardigrades Use Intrinsically Disordered Proteins to Survive
456   Desiccation. *Mol Cell* **65**, 975-984 e975, doi:10.1016/j.molcel.2017.02.018 (2017).
457 19   Malki, A. *et al.* Intrinsically Disordered Tardigrade Proteins Self-Assemble into
458   Fibrous Gels in Response to Environmental Stress. *Angew Chem Int Ed Engl* **61**,
459   e202109961, doi:10.1002/anie.202109961 (2022).
460 20   Arakawa, K. & Numata, K. Reconsidering the "glass transition" hypothesis of
461   intrinsically unstructured CAHS proteins in desiccation tolerance of tardigrades. *Mol*
462   *Cell* **81**, 409-410, doi:10.1016/j.molcel.2020.12.007 (2021).
463 21   Boothby, T. C. Water content influences the vitrified properties of CAHS proteins.
464   *Mol Cell* **81**, 411-413, doi:10.1016/j.molcel.2020.12.009 (2021).
465 22   Menze, M. A., Boswell, L., Toner, M. & Hand, S. C. Occurrence of mitochondria-
466   targeted Late Embryogenesis Abundant (LEA) gene in animals increases organelle
467   resistance to water stress. *J Biol Chem* **284**, 10714-10719,
468   doi:10.1074/jbc.C900001200 (2009).
469 23   Tanaka, S. *et al.* Novel mitochondria-targeted heat-soluble proteins identified in the
470   anhydrobiotic Tardigrade improve osmotic tolerance of human cells. *PLoS One* **10**,
471   e0118272, doi:10.1371/journal.pone.0118272 (2015).
472 24   Chakrabortee, S. *et al.* Intrinsically disordered proteins as molecular shields. *Mol*
473   *Biosyst* **8**, 210-219, doi:10.1039/c1mb05263b (2012).
474 25   Tolleter, D. *et al.* Structure and function of a mitochondrial late embryogenesis
475   abundant protein are revealed by desiccation. *Plant Cell* **19**, 1580-1589,
476   doi:10.1105/tpc.107.050104 (2007).
477 26   Tolleter, D., Hincha, D. K. & Macherel, D. A mitochondrial late embryogenesis
478   abundant protein stabilizes model membranes in the dry state. *Biochim Biophys*
479   *Acta* **1798**, 1926-1933, doi:10.1016/j.bbamem.2010.06.029 (2010).
480 27   Clarke, M. W. *et al.* Structural and Functional Insights into the Cryoprotection of
481   Membranes by the Intrinsically Disordered Dehydrins. *J Biol Chem* **290**, 26900-
482   26913, doi:10.1074/jbc.M115.678219 (2015).

12

483 28 Eddy, S. R. Accelerated Profile HMM Searches. *PLoS Comput Biol* **7**, e1002195,
484   doi:10.1371/journal.pcbi.1002195 (2011).
485 29 Zallot, R., Oberg, N. & Gerlt, J. A. The EFI Web Resource for Genomic
486   Enzymology Tools: Leveraging Protein, Genome, and Metagenome Databases to
487   Discover Novel Enzymes and Metabolic Pathways. *Biochemistry* **58**, 4169-4182,
488   doi:10.1021/acs.biochem.9b00735 (2019).
489 30 Tunnacliffe, A. & Wise, M. J. The continuing conundrum of the LEA proteins.
490   *Naturwissenschaften* **94**, 791-812, doi:10.1007/s00114-007-0254-y (2007).
491 31 Hundertmark, M. & Hincha, D. K. LEA (late embryogenesis abundant) proteins and
492   their encoding genes in Arabidopsis thaliana. *BMC Genomics* **9**, 118,
493   doi:10.1186/1471-2164-9-118 (2008).
494 32 Bies-Etheve, N. *et al.* Inventory, evolution and expression profiling diversity of the
495   LEA (late embryogenesis abundant) protein gene family in Arabidopsis thaliana.
496   *Plant Mol Biol* **67**, 107-124, doi:10.1007/s11103-008-9304-x (2008).
497 33 Bailey, T. L. & Elkan, C. Fitting a mixture model by expectation maximization to
498   discover motifs in biopolymers. *Proc Int Conf Intell Syst Mol Biol* **2**, 28-36 (1994).
499 34 Ohashi, Y. & Munro, S. Membrane delivery to the yeast autophagosome from the
500   Golgi-endosomal system. *Mol Biol Cell* **21**, 3998-4008, doi:10.1091/mbc.E10-05-
501   0457 (2010).
502 35 Wiedemann, N. & Pfanner, N. Mitochondrial Machineries for Protein Import and
503   Assembly. *Annu Rev Biochem* **86**, 685-714, doi:10.1146/annurev-biochem-060815-
504   014352 (2017).
505 36 Jensen, M. R., Zweckstetter, M., Huang, J. R. & Blackledge, M. Exploring free-
506   energy landscapes of intrinsically disordered proteins at atomic resolution using
507   NMR spectroscopy. *Chem Rev* **114**, 6632-6660, doi:10.1021/cr400688u (2014).
508 37 Kelley, L. A., Mezulis, S., Yates, C. M., Wass, M. N. & Sternberg, M. J. The Phyre2
509   web portal for protein modeling, prediction and analysis. *Nat Protoc* **10**, 845-858,
510   doi:10.1038/nprot.2015.053 (2015).
511 38 Wang, J., Sykes, B. D. & Ryan, R. O. Structural basis for the conformational
512   adaptability of apolipophorin III, a helix-bundle exchangeable apolipoprotein. *Proc
513   Natl Acad Sci U S A* **99**, 1188-1193, doi:10.1073/pnas.032565999 (2002).
514 39 Gautier, R., Douguet, D., Antonny, B. & Drin, G. HELIQUEST: a web server to
515   screen sequences with specific alpha-helical properties. *Bioinformatics* **24**, 2101-
516   2102, doi:10.1093/bioinformatics/btn392 (2008).
517 40 McLean, L. R., Hagaman, K. A., Owen, T. J. & Krstenansky, J. L. Minimal peptide
518   length for interaction of amphipathic alpha-helical peptides with phosphatidylcholine
519   liposomes. *Biochemistry* **30**, 31-37, doi:10.1021/bi00215a005 (1991).
520 41 Segrest, J. P. *et al.* The amphipathic helix in the exchangeable apolipoproteins: a
521   review of secondary structure and function. *J Lipid Res* **33**, 141-166 (1992).
522 42 Jumper, J. *et al.* Highly accurate protein structure prediction with AlphaFold. *Nature*
523   **596**, 583-589, doi:10.1038/s41586-021-03819-2 (2021).
524 43 Georgieva, E. R., Xiao, S., Borbat, P. P., Freed, J. H. & Eliezer, D. Tau binds to
525   lipid membrane surfaces via short amphipathic helices located in its microtubule-
526   binding repeats. *Biophys J* **107**, 1441-1452, doi:10.1016/j.bpj.2014.07.046 (2014).
527 44 Trexler, A. J. & Rhoades, E. Alpha-synuclein binds large unilamellar vesicles as an
528   extended helix. *Biochemistry* **48**, 2304-2306, doi:10.1021/bi900114z (2009).
529 45 Doherty, C. P. A. *et al.* A short motif in the N-terminal region of alpha-synuclein is
530   critical for both aggregation and function. *Nat Struct Mol Biol* **27**, 249-259,
531   doi:10.1038/s41594-020-0384-x (2020).
532 46 Williamson, J. A., Loria, J. P. & Miranker, A. D. Helix stabilization precedes
533   aqueous and bilayer-catalyzed fiber formation in islet amyloid polypeptide. *J Mol
534   Biol* **393**, 383-396, doi:10.1016/j.jmb.2009.07.077 (2009).

535 47 Buck, M. Trifluoroethanol and colleagues: cosolvents come of age. Recent studies
536 with peptides and proteins. *Q Rev Biophys* **31**, 297-355,
537 doi:10.1017/s003358359800345x (1998).
538 48 Jensen, M. R., Salmon, L., Nodet, G. & Blackledge, M. Defining conformational
539 ensembles of intrinsically disordered and partially folded proteins directly from
540 chemical shifts. *J Am Chem Soc* **132**, 1270-1272, doi:10.1021/ja909973n (2010).
541 49 Ozenne, V. *et al.* Flexible-meccano: a tool for the generation of explicit ensemble
542 descriptions of intrinsically disordered proteins and their associated experimental
543 observables. *Bioinformatics* **28**, 1463-1470, doi:10.1093/bioinformatics/bts172
544 (2012).
545 50 Holtzer, M. E. & Holtzer, A. Alpha-helix to random coil transitions: determination of
546 peptide concentration from the CD at the isodichroic point. *Biopolymers* **32**, 1675-
547 1677, doi:10.1002/bip.360321209 (1992).
548 51 Micsonai, A. *et al.* BeStSel: a web server for accurate protein secondary structure
549 prediction and fold recognition from the circular dichroism spectra. *Nucleic Acids*
550 *Res* **46**, W315-W322, doi:10.1093/nar/gky497 (2018).
551 52 Liu, W., Wang, Z., Fu, L., Leblanc, R. M. & Yan, E. C. Lipid compositions modulate
552 fluidity and stability of bilayers: characterization by surface pressure and sum
553 frequency generation spectroscopy. *Langmuir* **29**, 15022-15031,
554 doi:10.1021/la4036453 (2013).
555 53 Elderdfi, M. & Sikorski, A. F. Langmuir-monolayer methodologies for characterizing
556 protein-lipid interactions. *Chem Phys Lipids* **212**, 61-72,
557 doi:10.1016/j.chemphyslip.2018.01.008 (2018).
558 54 Camilleri, A. *et al.* Mitochondrial membrane permeabilisation by amyloid
559 aggregates and protection by polyphenols. *Biochim Biophys Acta* **1828**, 2532-2543,
560 doi:10.1016/j.bbamem.2013.06.026 (2013).
561 55 Huang, Z. & Tunnacliffe, A. Response of human cells to desiccation: comparison
562 with hyperosmotic stress response. *J Physiol* **558**, 181-191,
563 doi:10.1113/jphysiol.2004.065540 (2004).
564 56 Singh, J. *et al.* Transcriptional response of Saccharomyces cerevisiae to
565 desiccation and rehydration. *Appl Environ Microbiol* **71**, 8752-8763,
566 doi:10.1128/AEM.71.12.8752-8763.2005 (2005).
567 57 Pastor, M. M., Proft, M. & Pascual-Ahuir, A. Mitochondrial function is an inducible
568 determinant of osmotic stress adaptation in yeast. *J Biol Chem* **284**, 30307-30317,
569 doi:10.1074/jbc.M109.050682 (2009).
570 58 Pastore, D., Trono, D., Laus, M. N., Di Fonzo, N. & Flagella, Z. Possible plant
571 mitochondria involvement in cell adaptation to drought stress. A case study: durum
572 wheat mitochondria. *J Exp Bot* **58**, 195-210, doi:10.1093/jxb/erl273 (2007).
573 59 Gu, Z. *et al.* Aberrant cardiolipin metabolism in the yeast taz1 mutant: a model for
574 Barth syndrome. *Mol Microbiol* **51**, 149-158, doi:10.1046/j.1365-2958.2003.03802.x
575 (2004).
576 60 Yamaguchi, A. *et al.* Two novel heat-soluble protein families abundantly expressed
577 in an anhydrobiotic tardigrade. *PLoS One* **7**, e44209,
578 doi:10.1371/journal.pone.0044209 (2012).
579 61 Kikawada, T. *et al.* Dehydration-induced expression of LEA proteins in an
580 anhydrobiotic chironomid. *Biochem Biophys Res Commun* **348**, 56-61,
581 doi:10.1016/j.bbrc.2006.07.003 (2006).
582 62 Osman, C., Voelker, D. R. & Langer, T. Making heads or tails of phospholipids in
583 mitochondria. *J Cell Biol* **192**, 7-16, doi:10.1083/jcb.201006159 (2011).
584 63 Stepanyants, N. *et al.* Cardiolipin's propensity for phase transition and its
585 reorganization by dynamin-related protein 1 form a basis for mitochondrial

586   membrane fission. *Mol Biol Cell* **26**, 3104-3116, doi:10.1091/mbc.E15-06-0330
587   (2015).
588 64 Shi, Z., Graber, Z. T., Baumgart, T., Stone, H. A. & Cohen, A. E. Cell Membranes
589   Resist Flow. *Cell* **175**, 1769-1779 e1713, doi:10.1016/j.cell.2018.09.054 (2018).
590 65 Budin, I. *et al.* Viscous control of cellular respiration by membrane lipid
591   composition. *Science* **362**, 1186-1189, doi:10.1126/science.aat7925 (2018).
592 66 van Meer, G., Voelker, D. R. & Feigenson, G. W. Membrane lipids: where they are
593   and how they behave. *Nat Rev Mol Cell Biol* **9**, 112-124, doi:10.1038/nrm2330
594   (2008).
595 67 Bigay, J. & Antonny, B. Curvature, lipid packing, and electrostatics of membrane
596   organelles: defining cellular territories in determining specificity. *Dev Cell* **23**, 886-
597   895, doi:10.1016/j.devcel.2012.10.009 (2012).
598

Acknowledgments

Funding

Author contributions

X.-H.L. collected sequence data, wrote scripts and performed all the computational
analyses, made yeast strains, cloned the plasmids and purified proteins, performed CD,

fluorescence, biochemical, imaging, functional, and genetics experiments, C.W.H.Y. and S.M.V.F. performed the NMR experiments and corresponding analyses, N.G.-N. performed biochemistry experiments pertaining localization analyses, V.S. contributed to sample preparations and optimizations of liposome and functional assays, H.Z. performed the Langmuir-monolayer experiments under the supervision of W.L. and J.H., C.G. and B.L. performed experiments related to mitochondrial function under the supervision of M.M.B., M.K. and D.R.G. for helping with experiments and interpretation of mitochondrial functional analysis, A.M. helped with creating yeast strains used in the research, M.W. and K.M. contributed to establishment of the methodology of mitochondrial activity assays, C.M.J. contributed to the interpretation of biophysical characterizations, M.B. aided in computational analysis of disordered protein ensemble, B.S. aided in evolutionary analyses, E.A.M. contributed to design and optimization of yeast genetics experiments. X.-H.L., E.A.M., and M.M.B. designed the research, analyzed and interpreted the results, and wrote the manuscript; X.-H.L., C.W.H.Y., E.A.M., and M.M.B. contributed to data visualization. M.M.B. and X.-H.L. conceived, managed, and set the direction of the project. M.M.B. and E.A.M. co-supervised the project and S.M.V.F. co-supervised the NMR section of the project. All authors contributed to the editing of the manuscript.

Competing interests

The authors declare no competing interests.

Data and materials availability

All data are available in the manuscript or the supplementary materials; plasmids and strains described can be obtained from X.-H.L., E.A.M., or M.M.B.
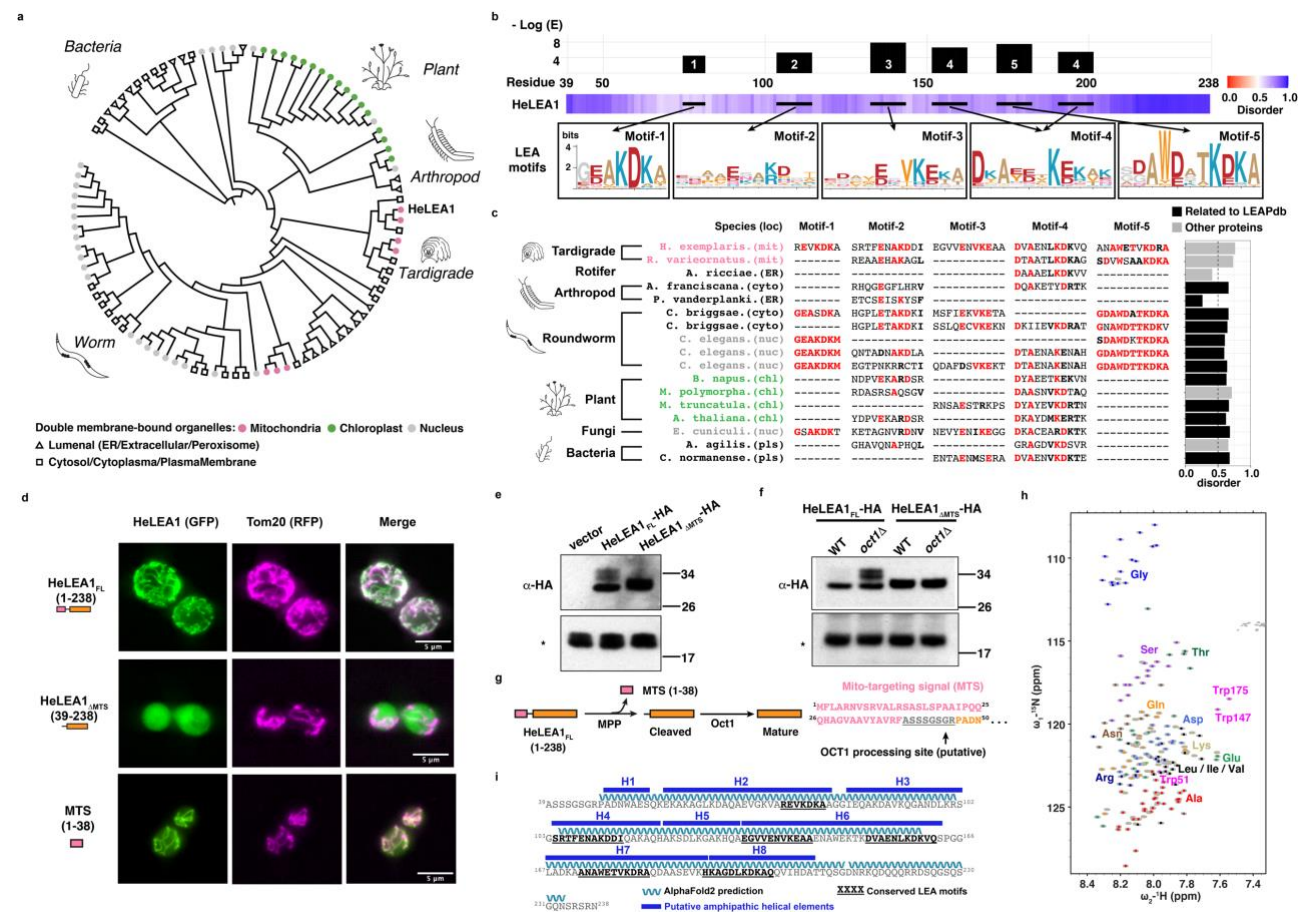
651

Fig. 1. HeLEA1 is an evolutionarily conserved IDP. a, Evolutionary tree of HeLEA1
homologs annotated by their predicted subcellular localization. Several HeLEA1 homologs
localize to various membrane-bound organelles. HeLEA1 was predicted to localize to the
mitochondria. **b,** HeLEA1 possesses multiple LEA protein motifs. Top panel shows
residue-specific confidence score of LEA motif in HeLEA1 (E score < 1E-4, MEME
algorithm[33]). Bottom panel shows disorder prediction for HeLEA1 using IUPred2A. The
locations of each high confidence motif are indicated by black lines, and the
corresponding motif logos shown below. **c,** Local motif alignments between HeLEA1 and
representative HeLEA1 homologs from diverse species and localizations. Mean disorder
score for each homolog are stacked on the right. Homologs related to the recorded entries
in the LEA protein database (LEAPdb) are highlighted in black. **d,** GFP-tagged (C-
terminal) full-length HeLEA1 (HeLEA1$_{FL}$-GFP) colocalized with mitochondria (marked by
Tom20-RFP) when expressed in yeast; removal of the N-terminal 38 amino acids
corresponding to the predicted MTS (HeLEA1$_{\Delta MTS}$-GFP) resulted in cytoplasmic
localization; fusing the predicted MTS to GFP also resulted in mitochondrial localization
(MTS-GFP). **e,** Immunoblottingimmunoblotting of log-phase cells expressing HA-tagged
HeLEA1$_{FL}$ revealed three species that likely correspond to full-length HeLEA1, MPP-
cleaved HeLEA1, and mature HeLEA1 with additional processing by mitochondrial
processing enzymes. HeLEA1$_{\Delta MTS}$-HA migrated as a single band of intermediate
molecular weight. **f,** Immunoblotting for HeLEA1$_{FL}$-HA and HeLEA1$_{\Delta MTS}$-HA in an *oct1Δ*
background demonstrated significant accumulation of processing intermediates only for
HeLEA1$_{FL}$, supporting its mitochondrial matrix localization. **g,** Proposed protein processing
events for HeLEA1 (orange): MTS (pink) is cleaved by MPP with the mitochondrial

17

675   intermediate peptidase Oct1 further processing N-terminal amino acids (grey). **h,** The

676    $^1H_N,^{15}N$ 2D HSQC of HeLEA1$_{\Delta MTS}$ purified from *E. coli* shown with assignment of

677   backbone resonances. Different types of amino acids are represented by different colours.

678   For full assignment of the HSQC spectrum please refer to **Extended Data Fig. 8**. **i,**

679   Locations of putative amphipathic helical elements predicted by biophysical properties

680   (blue), helical regions predicted by AlphaFold2 (cyan ribbons), overlapping with conserved
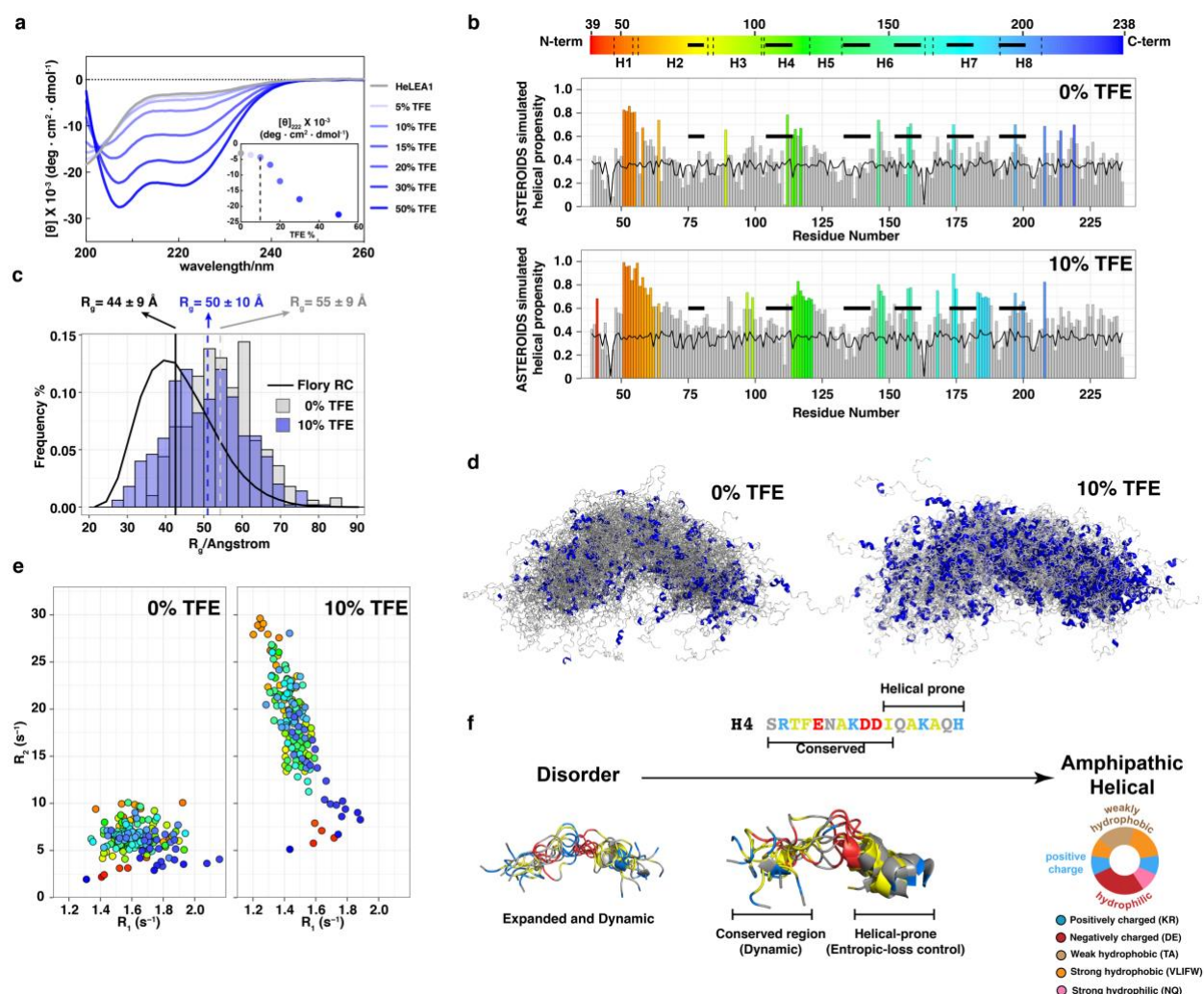
681   LEA motifs (black bold) in HeLEA1.

682

Fig. 2 Conserved elements of HeLEA1 remain dynamic during early stages of disorder-to-helical transition. a, Circular Dichroism (CD) Titration of 10μM HeLEA1 with trifluoroethanol (TFE). Inset shows the increase in helicity (monitored as molecular ellipticity at 222nm) as a result of increased TFE concentrations. Note that at 10% TFE (dashed line), HeLEA1 appears predominantly disordered. **b,** Residue-specific helical propensity based on *ASTEROIDS* fits of NMR data of HeLEA1 in 0% TFE (top) or 10% TFE (bottom). Residues with significant helical propensity (deviating > 0.3 from random coil (black line)) are highlighted according to the colour scheme on top. Black bars represent conserved LEA motifs mapped in **Fig. 1b. c,** Distribution of the radius of gyration (R_g) of the HeLEA1 ensemble generated assuming random coil (RC) behaviour (black line) or fitted with SAXS data either from 0% TFE (gray bars) or 10% TFE (blue bars). **d,** Full description of the conformational ensemble (100 representative conformers) of HeLEA1 in 0% TFE (left) and 10% TFE (right) by integrating NMR and SAXS data within the *ASTEROIDS* simulation pipeline. Helical regions in each conformer are highlighted in blue. **e,** Correlation maps of transverse (R_2) and longitudinal (R_1) relaxation rates of HeLEA1 in 0% (left) or 10% TFE. 10% TFE drastically increased the R_2 relaxation rates in regions with increased helical propensity, with same colour scheme as shown in **Fig. 2b. f.** Schematic depicting the disorder-to-helical transition for HeLEA1 H4 as an exemplar: weak amphipathic elements comprise a region of higher disorder propensity adjacent to a region with an increase in intrinsic helical propensity. This arrangement may

19

704   reduce the cost of conformational entropy during the disorder-to-helical transition. 10

705   conformers for the H4 region as predicted from *ASTEROIDS* ensembles are shown.
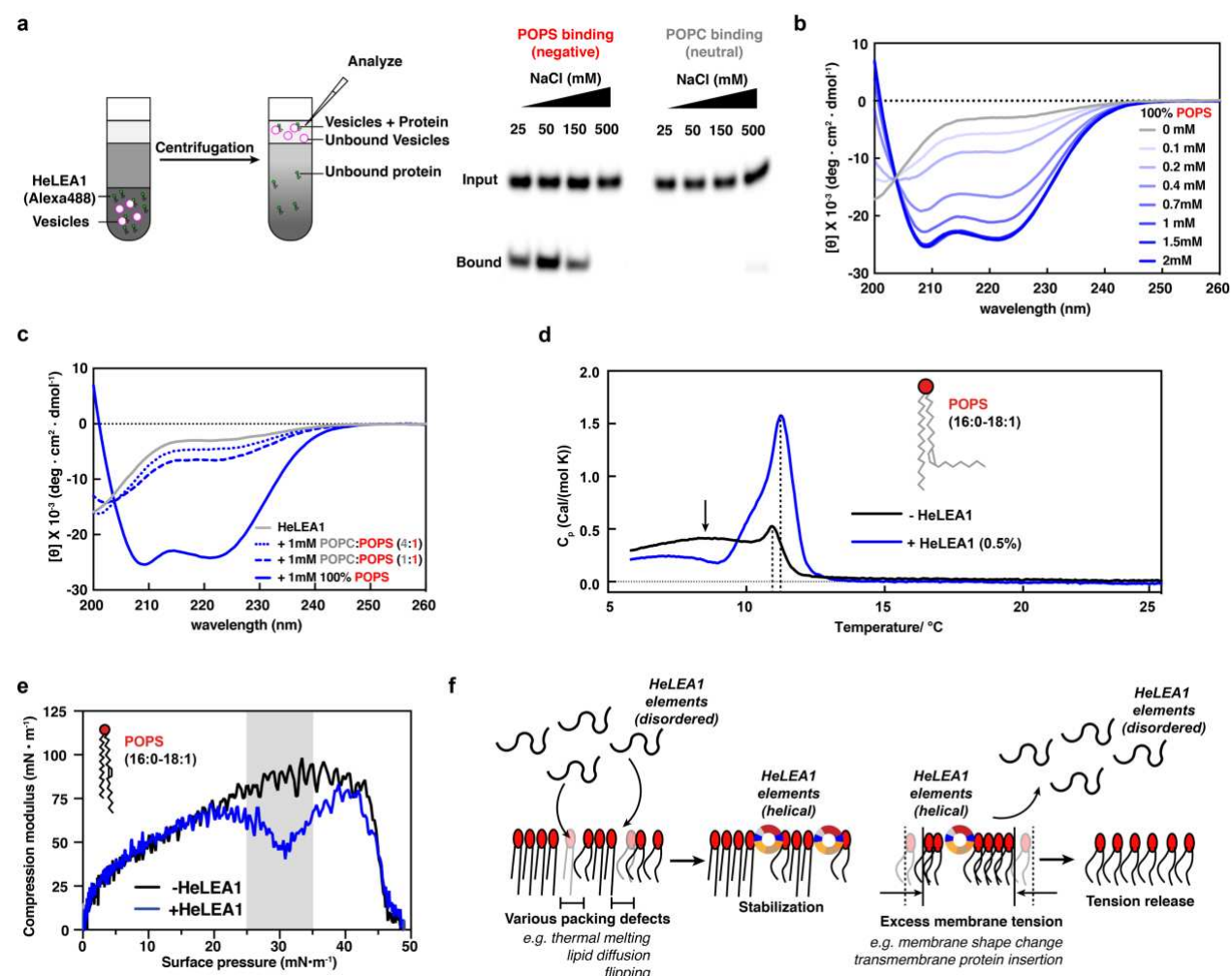
706

Fig. 3 HeLEA1 stabilizes negatively charged membranes through dynamic disorder-to-helical transition. a, Lipid flotation assay with Alexa Fluor 488–labelled HeLEA1 and liposomes made of various lipids (POPS, red; POPC, gray) at different salt concentrations. **b,** Titration of 10μM HeLEA1 with increasing amounts of 100% POPS SUVs monitored by CD. **c,** Titration of 10μM HeLEA1 with 1mM SUVs of different ratios of negatively charged POPS versus neutral POPC, monitored by CD. Decreasing the amount of POPS fraction significantly reduced the induced helicity of HeLEA1. **d,** Differential scanning calorimetry for POPS SUVs without (black line) and with HeLEA1 (0.5% molar ratio, blue line). HeLEA1 suppressed thermally induced phase transition at low temperature (broad peaks indicated by arrow) and increased phase transition temperature (peak position; dashed lines). **e,** Change of C_S^{-1} values in POPS monolayers with respect to surface pressure, as measured by Langmuir-monolayer methodology, with or without 3nM HeLEA1 (1:50 protein:lipid ratio). Gray areas depict the range of physiological surface pressure. **f,** Proposed mechanism for the molecular function of HeLEA1. A disorder-to-helical transition occurs within putative amphipathic elements in HeLEA1 when HeLEA1 interacts with negatively charged lipids at areas of the membrane with lipid packing defects, resulting in stabilization (left). When excess surface tension occurs at a HeLEA1-bound membrane, HeLEA1 elements would unfold and detach from the membrane to buffer such tension, stabilizing the membrane and increasing membrane fluidity (right).
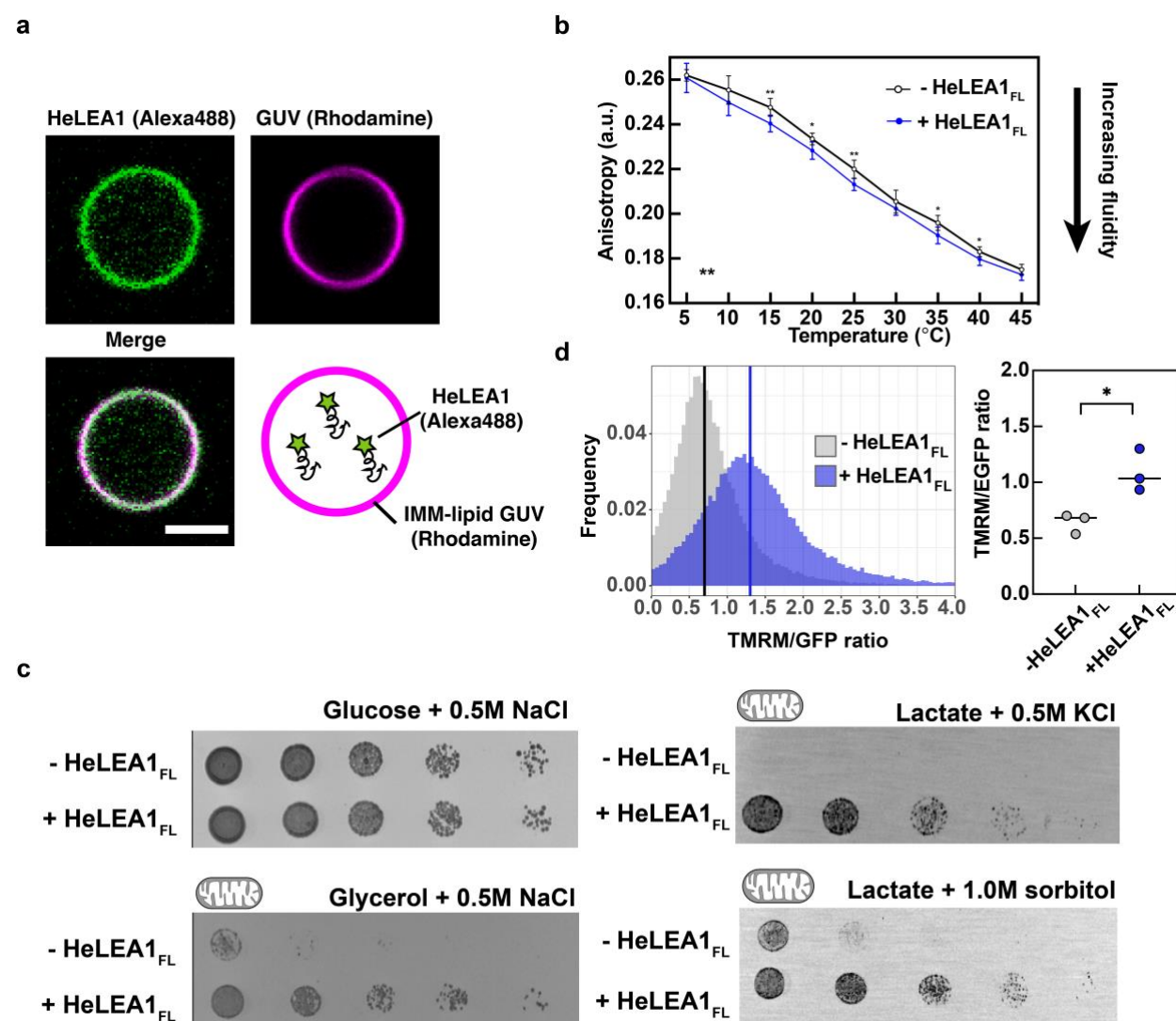
21

Fig. 4 Physiological impact of HeLEA1 expression. a, Confocal imaging showing colocalization of HeLEA1 and GUVs with a composition mimicking that of the inner mitochondrial membrane (IMM). GUVs were labelled with DOPE-Lissamine rhodamine (magenta). HeLEA1 was labelled with Alexa Fluor 488 (green) and encapsulated inside GUVs. Scale bar: 3 μm. **b,** Temperature-dependent fluorescence anisotropy of DPH-stained mitochondria from yeast cells grown in normal YPD media. Mitochondria with HeLEA1$_{FL}$ expression had lower anisotropy than without HeLEA1$_{FL}$ expression (**, $P <$ 0.01, two-way ANOVA, $n = 7$, error bars represent the standard deviation), suggesting that HeLEA1$_{FL}$ expression increases the membrane fluidity of mitochondria. For each temperature pairs, an independent unpaired t-test were also performed, and the statistical significance was indicated (*, $P < 0.05$, **, $P < 0.01$, two-tailed, unpaired t-test, $n = 7$). **c,** HeLEA1$_{FL}$ expression had a positive fitness effect on various hyperosmotic stress when cells were grown on non-fermentable carbon sources, in which mitochondrial activity is crucial for cell survival, but not with fermentable carbon source glucose where mitochondrial activity is less critical for survival. **d,** Normalized TMRM fluorescence for yeast cells with or without HeLEA1$_{FL}$ expression grown on glycerol. HeLEA1$_{FL}$ expression significantly increase mitochondrial membrane potential, suggesting enhanced

746   mitochondrial activity in live cells. Representative FACS data for one replica (left, lines

747   indicate median of the distribution) and statistical test for three independent replica (*, $P <$

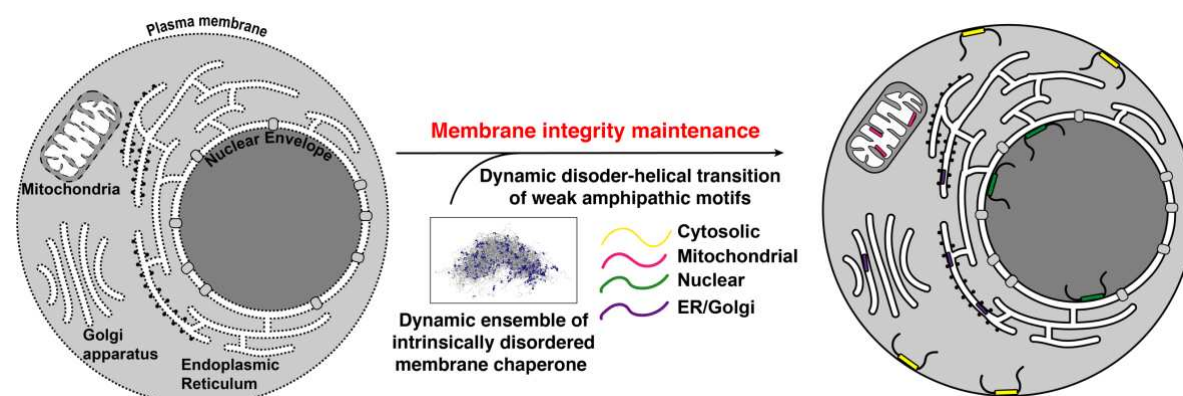748   0.05, Welch t-test, $n = 3$, right) are shown.

749

Fig. 5 Proposed function for HeLEA1 homologs. HeLEA1 homologs may confer various stress tolerance phenotype by acting as membrane chaperones targeted to different subcellular localizations.